Dyes and Pigments 84 (2010) 190–202

Contents lists available at ScienceDirect

Dyes and Pigments

journal homepage: www.elsevier.com/locate/dyepig

Electroluminescence and photovoltaic properties of light-emitting devices and solar cells comprising 2-pyran-4-ylidene-malononitrile conjugated polymers

Rong-Ho Lee*, Li-Wei Liu

Department of Chemical and Materials Engineering, National Yunlin University of Science & Technology, Yunlin 640, Taiwan, R.O.C

ARTICLE INFO

Article history:
Received 25 June 2009
Received in revised form
10 August 2009
Accepted 11 August 2009
Available online 27 August 2009

Keywords:
Conjugated polymer
Hyper-branched polymer
Electroluminescence
Polymer light-emitting display
Photovoltaic property
Polymer solar cell

ABSTRACT

Several main-chain type and triazine-branched, fluorene and thiophene copolymers containing a 2-pyran-4-ylidene-malononitrile derivative were synthesized using the Suzuki coupling reaction. A triazine-branched fluorene-based device displayed superior electroluminescence performance with a brightness $\leq$1031 cd m^{-2} and an efficiency of 1.97 cd A^{-1}. A polymer solar cell, comprising an interpenetrating network of conjugated polymer as electron donor and a fullerene derivative, (6,6)-phenyl-C_{61}-butyric acid methyl ester, as the electron acceptor, exhibited photocurrent density and photo-energy conversion efficiency of 5.07 mA cm^{-2} and 0.50%, respectively.

1. Introduction

Conjugated polymers consisting of an electronically delocalized backbone are significant technological materials that enjoy much usage in optoelectronics, such as in polymer light-emitting devices (PLEDs) and polymer solar cells (PSCs) [1–4]. PLEDs have been the focus of extensive research for flat-panel display devices, owing to their low turn-on voltage, high brightness, high efficiency, easy processing and low-cost fabrication [1,2]. In PLED's, electrons and holes are injected from the cathode and anode, respectively, these being driven by the applied electric field. The charge carriers move through the polymer layer over a certain distance until recombination occurs; such recombination of electrons and holes is responsible for the electroluminescence (EL) of PLEDs [1,2]. In addition, PSCs are a promising alternative to conventional inorganic solar cells owing to their large area, flexible shape, low mass, ease of processing and low-cost fabrication [3,4]. The conversion of solar light into electrical power requires the generation of both electrons and holes and a potential that extracts these charges to an external circuit. To obtain efficient photon-to-charge conversion, many different PSC architectures have been developed, such as single-layer cells [5], double-layer cells [6], and bulk-hetero-junction (BHJ) blend cells [7–10].

High brightness, great current efficiency, and good color purity are required for the application of PLEDs in a flat-panel display. For a PLED to display high brightness and high efficiency requires optimum charge transport and balance throughout the light-emitting layer [11,12], which is determined by the chemical structure of the light emitting polymer (LEP). The bipolar characteristics of light emitting polymer containing electron- and hole-transporting moieties are responsible for carrier transport and balance throughout the light-emitting layer and, as such, can be used to enhance the brightness and efficiency of PLEDs [13–17]. Despite their promise, the application of conjugated polymers in PLEDs has been hampered because by the formation of an undesired long-wavelength excimer emission band [18–27]. Excimer emission from aggregates formed by polymer chain $\pi-\pi$ stacking in conjugated polymer polymers usually results in low efficiency and poor colour purity [18–27]. A light emitting polymer with a hyper-branched structure shows reduced aggregation and excimer formation [28–30]; moreover, a hyper-branched light emitting polymer with electron- or hole-conducting groups as branching units, has been shown to enhance the charge injection and transpor properties of PLEDs, in addition to displaying reduced excimer effect [31–33].

In the case of PSCs, the major advances in solar energy conversion efficiency have been accomplished by replacing the double-layer cell with a BHJ blend for the photoactive layer [7–10]. Unlike

* Corresponding author. Tel.: +886 5 5342601x4625; fax: +886 5 5312071.
E-mail address: lerongho@yuntech.edu.tw (R.-H. Lee).

0143-7208/$ – see front matter © 2009 Elsevier Ltd. All rights reserved.
doi:10.1016/j.dyepig.2009.08.002

the double-layer cell, the BHJ is able to circumvent the limitation of the charge generation by means of a two-dimensional network of photo-induced charge-generating interfaces. In most BHJ cells, the photoactive layer is based on a blend of an electron-donor polymer and an electron-acceptor fullerene derivative, [6,6]-phenyl-C_{61}-butyric acid methyl ester (PCBM)) [7–10]. Electron-donating polymers such as poly(2-methoxy-5-(2′-ethyl-hexyloxy)-1,4-phenylenevinylene), poly(2-methoxy-5-(3,7-dimethyloctyloxy)-1,4-phenylene vinylene), and poly(3-hexylthiophene) have been employed as the electron-donor in PSCs [7–10,34–36]. The choice of PCBM as electron-acceptor is critical in order to obtain sufficient transport of electrons [7–10,34–36]. For PSCs, a conjugated polymer with a suitable combination of optical, electrochemical and electronic properties would favorable for efficient photon-to-charge conversion. A conjugated polymer with a low-band gap is crucial for harvesting more solar radiation [37–39] and high charge mobility of the polymer is also required for high current density in PSCs [38–40]. In addition to the intrinsic characteristics of the polymer, the amount of PCBM in a blend [41,42], the compatibility of the polymer and PCBM, the morphology of the photoactive layer [9,43] and device processing conditions also play important roles in the photovoltaic (PV) performance of PSCs [35,44,45]. The efficiency of conjugated polymer/PCBM-based PSCs has been shown to depend on processing conditions and can be improved using a thermal annealing treatment of the photoactive layer. Accurate control of annealing conditions is essential to gain excellent PV performance in PSCs [35,44,45].

This work concerns the synthesis, using the Suzuki coupling reaction, of two, main-chain type, fluorene and thiophene copolymers (MPFM and MPTM) which contain a 2-pyran-4-ylidene-malononitrile (PM) derivative; in addition, two triazine-branched, fluorene and thiophene copolymers (HPFM and HPTM) containing the PM moiety were also synthesized (Fig. 1). As a low-band gap polymer with high charge mobility is ideal as the donor polymer in preparing a PSC with efficient photon-to-charge conversion, novel, low-band-gap PM-containing copolymers were developed. As PM-containing polymers are well known for their use as red-emitters in PLEDs [46–49], the electroluminescence properties of PLEDs containing these PM-copolymers were also studied. The electron-donor moieties, fluorene and thiophene, were copolymerized with the electron-deficient PM moiety, and the ensuing copolymers therefore had a bipolar structure within the polymer backbone. As excellent EL or PV properties are expected for PLEDs or PSCs fabricated from such bipolar conjugated polymers [50,51], the effects of the hyper-branched structure on the EL and PV properties of PLEDs and PSCs based on the triazine-branched, fluorene and thiophene copolymers (HPFM and HPTM) were also investigated. In addition, the effects of thermal treatment on the morphology and PV properties of the main-chain and triazine-branched polymers based PSCs was also examined in detail.

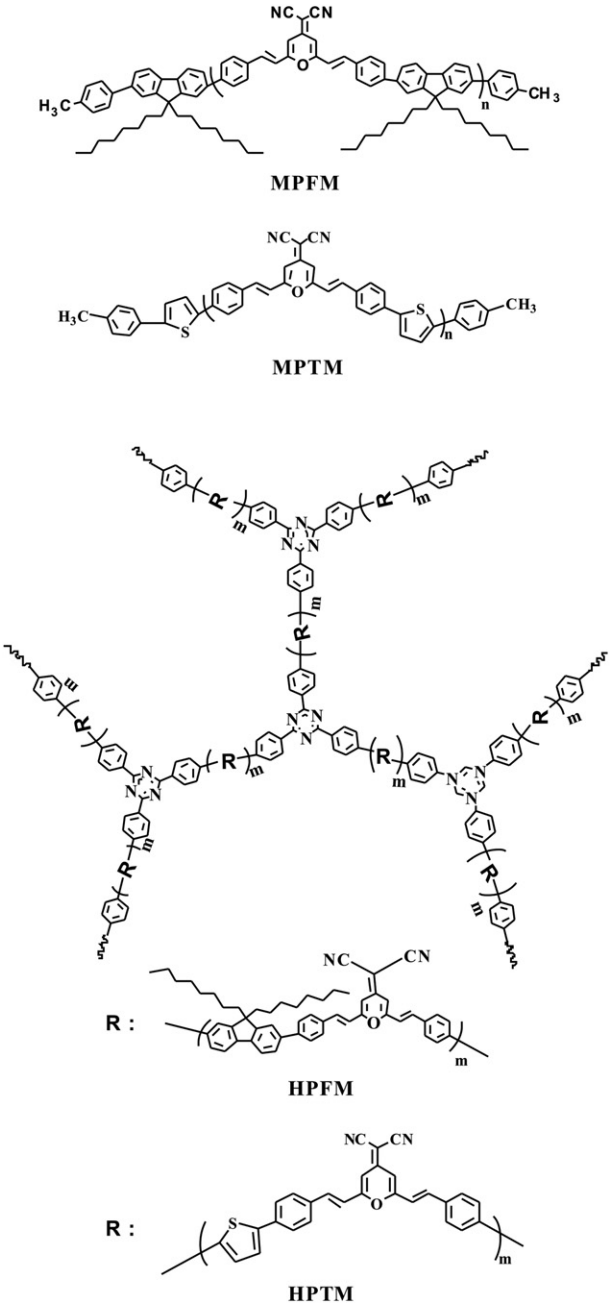

Fig. 1. Chemical structures of the main-chain type and triazine-branched conjugated polymers.

2. Experimental section

2.1. Synthesis of main-chain type and hyper-branched conjugated polymers

All reactions and manipulations were performed under a nitrogen atmosphere using standard Schlenk techniques. All chromatographic separations were carried out on silica gel. Toluene and tetrahydrofuran (THF) were distilled over sodium/benzophenone in a nitrogen atmosphere. Chloroform was dried over CaH_2. Chemicals were reagent grade and purchased from Aldrich, Fluka, Sigma, and RDH Chemical Co. All chemicals were used as-received unless otherwise described. 2,7-Bis(4,4,5,5-tetramethyl-1,3,2-dioxaborolan-2-yl)-9,9-dioctylfluorene (compound 1), 2,5-Bis(4,4,5,5-tetramethyl-1,3,2-dioxaborolan-2-yl)-thiophene (compound 2), 2-{2,6-bis[2-(4-bromophenylene)vinyl]pyran-4-ylidene} malononitrile (compound 3) and 2,4,6-tris-(4-bromophenyl)-[1,3,5]triazine (compound 4) were synthesized as previously described [33,46]. All polymers were prepared through the palladium-catalyzed Suzuki coupling polymerization. The structure of the conjugated polymers was identified using ^{1}H NMR spectroscopy. The average M_r of the polymers was determined using gel permeation chromatography (GPC).

2.1.1. Polymerization of main-chain type MPFM

For MPFM, compound 1 (2 g, 3.11 mmol), compound 3 (1.58 g, 3.11 mmol), and tetrakis(triphenylphosphine) palladium (0) ($Pd(PPh_3)_4$, (caution: incompatible with moist air or water, strong

oxidants; hazardous decomposition products) 0.06 g, 0.052 mmol %) were dissolved in a mixture of toluene (100 mL) and aqueous K_2CO_3 (2.76 g in 10 mL H_2O). The solution was refluxed with vigorous stirring under a nitrogen atmosphere for 24 h and 4-bromo-toluene (0.6 mL, 0.7 mmol), was added to the reaction mixture together with additional $Pd(PPh_3)_4$ and reaction was continued for a further 24 h. The ensuing mixture was poured into methanol (200 mL) and the precipitate was removed by filtration. The polymer was dissolved in a small amount of THF and precipitated in methanol several times. The purified polymer was filtered and dried under vacuum. The yield of yellow solid powder MPFM was 56% (1.5 g). M_n = 23.0 kg/mol; M_w = 23.7 kg/mol ^{1}H NMR (600 MHz, $CDCl_3$): δ[ppm]: 0.81(m,10H), 1–1.22 (m, 20H), 2–2.1 (m, 10H), 6.7–6.8 (s, 2H), 6.8–6.9 (d, 2H), 7.4–7.5 (m, 6H), 7.56–7.62 (d, 4H), 7.74–7.8 (d, 2H), 7.8–7.85 (s, 2H), 7.96–8.0 (d, 2H). Elemental analysis found: C, 87.74%; H, 7.19%; O, 2.01%; and N, 3.54%.

2.1.2. Polymerization of triazine-branched HPFM

For HPFM, compound 1 (1.5 g, 2.33 mmol), compound 3 (1.0 g, 1.98 mmol), compound 4 (0.14 g, 0.26 mmol) and $Pd(PPh_3)_4$, (0.06 g, 0.052 mmol %) were dissolved in a mixture of toluene (100 mL) and aqueous K_2CO_3 (2.76 g in 10 mL H_2O). The solution was refluxed with vigorous stirring under a nitrogen atmosphere for 24 h and 4-bromo-toluene (0.6 mL, 0.7 mmol), was added together with additional $Pd(PPh_3)_4$ and reaction continued for a further 24 h. The reaction and purification procedures were the same as those for MPFM. The yield of yellow solid powder HPFM was 56% (1.0 g). M_n = 30.6 kg/mol; M_w = 34.1 kg/mol ^{1}H NMR (600 MHz, $CDCl_3$): δ[ppm]: 0.81(m, 10H), 1–1.22 (m, 20H), 2–2.2 (m, 10H), 6.7–6.68 (s,2H), 6.8–6.9 (d, 2H), 7.2–7.5 (m, 4H), 7.58–7.68 (m, 6H), 7.68–7.74 (d, 4H), 7.75–7.80 (d, 2H), 7.8–7.84 (s, 2H), 7.98–8.0 (d, 2H). Elemental analysis found: C, 87.09%; H, 6.75%; O, 1.92%; and N, 4.18%.

2.1.3. Polymerization of main-chain type MPTM

For MPTM, compound 2 (1 g, 2.84 mmol), compound 3 (1.4 g, 2.76 mmol), and tetrakis(triphenylphosphine) palladium (0) ($Pd(PPh_3)_4$, 0.05 g, 0.043 mmol) were dissolved in a mixture of toluene (100 mL) and aqueous K_2CO_3 (2.76 g in 10 mL H_2O). The solution was refluxed with vigorous stirring under a nitrogen atmosphere for 24 h and 4-bromo-toluene (0.6 mL, 0.7 mmol) was added to the reaction mixture together with additional $Pd(PPh_3)_4$ and reaction continued for a further 24 h. The reaction and purification procedures were the same as those of MPFM. The yield of red solid powder MPTM was 57% (1.5 g). M_n = 16.7 kg/mol; M_w = 17.5 kg/mol ^{1}H NMR (600 MHz, $CDCl_3$): δ[ppm]: 1.25(s, 6H), 6.7(s, 2H), 6.72–6.74 (d, 2H), 7.1–7.12 (d, 4H), 7.33–7.35 (d, 4H), 7.41–7.45 (m, 6H), 7.55–7.59 (d, 4H), 7.66–7.7 (s, 2H). Elemental analysis found: C, 83.11%; H, 3.91%; O, 3.60%; N, 6.38%; S, 3.31%.

2.1.4. Polymerization of triazine-branched HPTM

For HPTM, compound 2 (1.2 g, 3.57 mmol), compound 3 (1.8 g, 3.55 mmol), compound 4 (0.21 g, 0.38 mmol), and $Pd(PPh_3)_4$, (0.06 g, 0.052 mmol %) were dissolved in a mixture of toluene (100 mL) and aqueous K_2CO_3 (2.76 g in 10 mL H_2O). The solution was refluxed with vigorous stirring under a nitrogen atmosphere for 24 h and 4-bromo-toluene (0.6 mL, 0.7 mmol), was added to the reaction mixture together with additional $Pd(PPh_3)_4$ and reaction continued for a further 24 h. The reaction and purification procedures were the same as those of MPFM. The yield of red solid powder HPTM was 57% (1.02 g). M_n = 16.7 kg/mol; M_w = 16.9 kg/mol ^{1}H NMR (600 MHz, $CDCl_3$): δ[ppm]: 6.7 (s, 2H), 6.7–6.8 (d, 2H), 7.1 (d, 2H), 7.34 (d, 2H), 7.4–7.46 (m, 6H), 7.48–7.52 (d, 4H), 7.54–7.58 (d, 4H), 7.65–7.7 (d, 2H). Elemental analysis found: C, 81.3%; H, 4.74%; O, 3.69%; N, 7.54%; S, 3.51%.

2.2. Instruments

^{1}H NMR spectra were recorded on a Bruker AMX-600 MHz Spectrometer. The elemental analysis was carried out with an elemental analyzer (Elementar Vario EL III). GPC measurements were carried out on a Waters chromatography instrument (Waters, 717 plus Autosampler). Two Waters Styragel linear columns were used, with polystyrene as the standard and THF as the eluent. Glass transition temperatures (T_g) were measured by differential scanning calorimetry (DSC: TA Instruments, DSC-2010) in a nitrogen atmosphere at a heating rate of 10 °C/min. Thermogravimetric analysis (TGA) of the polymer was performed in a nitrogen atmosphere at a heating rate of 10 °C/min by using a Thermogravimetric Analyzer (TA Instruments, TGA-2050). The UV–Vis spectrum was measured using a Hewlett–Packard 8453 with a photodiode array detector. Photoluminescence (PL) and EL spectra were recorded on a Hitachi F-4500 fluorescence spectrophotometer. Redox potentials of the polymers were determined by cyclic voltammetry (CV) using a BAS 100B electrochemical analyzer with a scanning rate of 100 mV/s. The polymer was dissolved in deoxygenated dry dimethylformamide with 0.1 M tetrabutylammonium perchlorate as the electrolyte. A platinum working electrode and a saturated non-aqueous $Ag/AgNO_3$ reference electrode were used. Ferrocene was used for potential calibration (all reported potentials are referenced against Ag/Ag+) and for reversibility criteria. The morphology of the polymer solid films was studied using an atomic force microscope (AFM; Digital Instrument: Dimension 3100 Series Scanning Probe Microscope).

2.3. EL device fabrication and characterization

The PLED structure in this study was indium tin oxide (ITO))-coated glass/hole-transporting material (HTM)/LEP/Ca (10 nm)/Al (100 nm). ITO-coated glass, with a sheet resistance of 15 Ω/square, was purchased from Applied Film Corp. Glass substrates with patterned ITO electrodes were cleaned using O_2 plasma treatment. A thin film (600 Å) of HTM poly(3,4-ethylenedioxythiophene) doped with poly(styrenesulfonate) (PEDOT:PSS, AI4083, Bayer) was formed on the ITO layer of a glass substrate by the spin-casting method. Light-emitting layers were then spin-coated (1500 rpm) from the LEP solutions (15 mg/mL) onto the HTM layer, and dried at 80 °C for 1 h in a glove box. LEP solutions were prepared with cyclohexanone (CHO) or CHO/THF (1:1 by volume). A high-purity calcium (Ca) cathode was thermally deposited onto the LEP thin film, followed by silver (Ag) metal deposition as the top layer, in a high-vacuum chamber. After electrode deposition, the PLED was transferred from the evaporation chamber to a glove box purged by high-purity nitrogen gas to keep oxygen and moisture levels below 1 ppm. The device was then encapsulated by glass covers sealed with UV-cured epoxy glue in the glove box. The cathode deposition rate was determined with a quartz thickness monitor (STM-100/MF, Sycon). Thin-film thickness was determined with a surface texture analysis system (3030ST, Dektak). Current-voltage characteristics were measured on a programmable electrometer with current and voltage sources (Keithley 2400). Luminance was measured with a BM-9 luminance meter (Topcon).

2.4. PSC device fabrication and characterization

The PSC fabrication was based on an interpenetrating network of conjugated polymer and fullerene derivative (PCBM.). The PCBM was purchased from ADS (American Dye Source Corp.) and used as received. Solutions (30 mg/mL) of the conjugated polymer and PCBM in different weight ratios were prepared with CHO or CHO/THF (1:1 by volume). PSCs were prepared by the following

procedure: Glass substrates with patterned ITO electrodes were well washed then cleaned by O_2 Plasma treatment. A thin film of HTM was formed on the ITO layer of a glass substrate by the spin-casting method. The conjugated polymer: PCBM composite film was spin-coated (1500 rpm) from the CHO or CHO/THF solution onto the HTM layer and was dried at 80 °C for 1 h in a glove box. The LiF/Al-based cathode was thermally deposited onto the conjugated polymer/PCBM composite-based photoactive thin film in a high-vacuum chamber. The active area of the PSC was 0.04 cm^2. After the electrode deposition, the PSC was encapsulated as well as the PLED. The PV properties of the PSCs were measured on a programmable electrometer with current and voltage sources (Keithley 2400) under the illumination of a 100 mW/cm^2 solar light from an AM1.5 solar simulator (NewPort Oriel 96 000, Solar simulator).

3. Results and discussion

3.1. Chemical structure characterization and thermal properties of the polymers

The chemical structures of the conjugated polymers were characterized by ^1H NMR spectroscopy. The chemical shifts and the relative intensities of the signals are in agreement with the proposed structures for the conjugated polymers. The number and weight average molecular weight of the fluorene/PM-containing polymers (MPFM and HPFM) were about 22.0–30.0 and 23.0–34.0 kg/mol, respectively. For the thiophene/PM-containing polymers (MPTM and HPTM), the number and weight average molecular weight were about 16.5–16.9 and 16.0–17.0 kg/mol, respectively. Fluorene/PM-containing polymers show a higher molecular weight than the thiophene/PM-containing polymers. For the triazine-branched PM-containing copolymers, the ^1H NMR spectra reveal that the average repeat unit of PM in one arm is approximately three for both HPFM and HPTM. According to the weight average molecular weight, two to three generations on average were observed for both HPFM and HPTM. In addition, the solubility of the conjugated polymers in organic solvents was also studied. Fluorene/PM-containing polymers are soluble in most of the organic solvents, such as CHO, THF, chloroform, dichloromethane, and dichlorobenzene. In contrast, the thiophene/PM-containing polymers are less soluble in most of the organic solvents even through the thiophene/PM-containing polymers have a lower molecular weight than the fluorene/PM-containing polymers. Fluorene, with a long alkyl side chain, exhibits a better solubility than thiophene. Consequently, fluorene/PM-containing polymers show a better solubility than thiophene/PM-containing polymers. Furthermore, the hyper-branched structure was favorable for the solubility enhancement of triazine-based conjugated polymers. Therefore, better solubility was observed for the HPTM in comparison with MPTM. HPTM is soluble in CHO, THF, chloroform, dichloromethane, and dichlorobenzene. On the other hand, thermal stability of conjugated polymers plays an important role in the operating stability of optoelectronic devices. Operational stability of optoelectronic devices such as PLEDs and PSCs is directly related to the thermal stability of the conjugated polymer. Thus, a high T_g and high thermal degradation temperature are favorable for the application of a conjugated polymer in outdoor displays or solar cells. The glass transition temperatures of the conjugated polymers MPFM, HPFM, MPTF, and HPTM were found at around 138.5, 142.1, 122.6, and 125.9 °C, respectively. These results indicate that the fluorene/PM-containing polymers show a higher T_g than the thiophene/PM-containing polymers. This can be attributed to the much higher molecular weight of the fluorene/PM-containing polymers as compared to those of the thiophene/PM-containing polymers. In addition, the temperatures at which five percent weight loss occurs for the conjugated polymers MPFM, HPFM, MPTM, and HPTM were found to be approximately 380, 396, 340, and 350 °C, respectively. Fluorene/PM-containing polymers show a higher thermal stability than the thiophene/PM-containing polymers.

3.2. Optical properties of the polymers

The normalized UV–vis absorption spectra of PM and conjugated polymers in solution and as solid films are shown in Fig. 2. In Fig. 2(a), PM in CHO shows a maximal absorption peak at 413 nm with corresponding additional absorption peaks at 390, 436, and 465 nm. For fluorene/PM-containing polymers, a 24 nm red shift of the maximal absorption peak was observed for MPFM and HPFM as compared to PM, indicating the effect of incorporation of the fluorene moiety on the electronic band gap of the polymers. Moreover, higher absorption intensity was observed in the range of 350–380 nm for the HPFM as compared to the MPFM, due to the absorption of the triazine unit. In addition, the UV–vis absorption behavior of MPTM was studied by while dissolved in a CHO/THF co-solvent mixture (1:1 by volume) due to the poor solubility of MPTM in CHO. The absorption behaviors of MPTM and HPTM were similar to that of PM. The red-shifting of absorption peaks was not significant for the thiophene/PM-containing polymers in comparison with PM. In Fig. 2(b), a red shift and a full-width at half-maximum (FWHM) enhancement of the absorption peaks were observed for the polymers in solid film form as compared to those

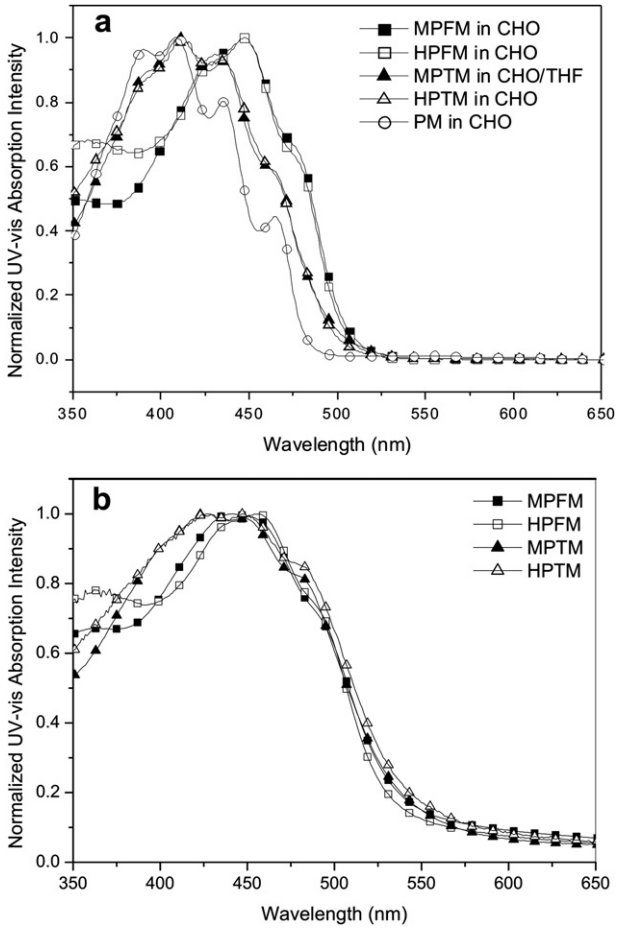

Fig. 2. Normalized UV–vis absorption spectra of the conjugated polymers ((a) in solution; and (b) as a solid film).

in solution. These results were attributed to the interaction and aggregation between the polymer chains. Moreover, the red-shift of the absorption peaks was more significant for the thiophene/PM-containing polymers as compared to the fluorene/PM-containing polymers. Therefore, the absorption spectra of the MPTM and HPTM almost overlapped with the spectra of MPFM and HPFM.

The PL spectra of the polymers in solution and as solid film are shown in Fig. 3. For the fluorene/PM-containing polymers, the PL emission maximal of MPFM and HPFM in solution was observed at 545 and 539 nm, respectively. A red shift and a broadening of the emission peaks were observed for the MPFM and HPFM in solid film as compared to the polymer solutions, due to the inter-chain aggregation formation in the polymer film. Moreover, the maximal PL emission wavelength of the triazine-branched polymer, HPFM was shorter than the main-chain polymer, MPFM due to the short conjugation length of the chain segment between the two branching units in HPFM. On the other hand, thiophene/PM-containing polymers with a low band-gap showed a longer PL emission maximum than the fluorene/PM-containing polymers. For the MPTM as solid film, the PL emission maximum was observed at around 585 nm, with a 35 nm red-shift from the PL in solution. Moreover, the triazine-branched polymer HPTM in solution showed a main emission peak at 525 nm, accompanied by a shoulder emission at around 600 nm. A pronounced red shift of PL emission was observed for HPTM as a solid film in comparison with HPTM in solution. Furthermore, the FWHMs of the PL emission peaks were reduced significantly for the thiophene/PM-containing polymers as a solid film in comparison with those in solution. The solvate-chromic effect is responsible for FWHM reduction of the PL emission band.

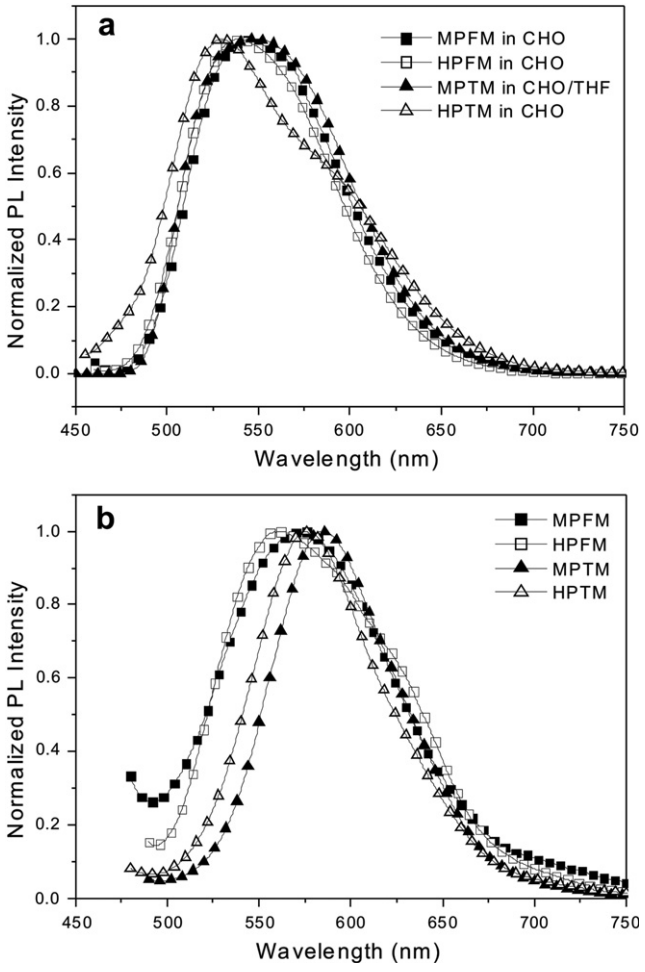

Fig. 3. Normalized PL spectra of the conjugated polymers ((a) in solution; (b) as a solid film; excitation wavelength: 380 nm).

3.3. Electrochemical properties

CV was employed to investigate the electrochemical behavior and to estimate the highest occupied molecular orbital (HOMO) and lowest unoccupied (LUMO) energy levels of the conjugated polymers. The HOMO energy level of the polymers was calculated from the onset potential of oxidation by assuming the absolute energy level of ferrocene is −4.71 V below the vacuum level, and the LUMO energy level was calculated from the HOMO energy level and the absorption edge [52–54]. The electrochemical properties of polymers are summarized in Table 1. Cyclic voltammograms show that oxidation onset potentials (E^{ox}_{onset}) were observed at 0.60 and 0.57 V for MPFM and HPFM, respectively. Optical band gaps of MPFM and HPFM, determined from the absorption edge, were 1.98 and 1.94 eV, respectively. LUMO levels of MPFM and HPFM were −3.33 and −3.34 eV, respectively, while HOMO levels were −5.31 and −5.28 eV, respectively. Unlike MPFM having a larger band gap, the incorporation of the electron-deficient unit, triazine led to a lower LUMO level and a higher HOMO level for HPFM [31]. The conjugated polymer possessed a lower LUMO level, allowing for efficient electron-injection from a cathode in a PLED application. The polymer with a higher HOMO level was favorable for an efficient hole-injection from an ITO transparent anode. Therefore, the EL properties would be enhanced for a PLED based on such a conjugated polymer. On the other hand, E^{ox}_{onset} values were observed at 0.35 for MPTM and 0.25 V for HPTM. Optical band gaps of MPTM and HPTM, determined from the absorption edge, were 1.89 and 1.65 eV, respectively. LUMO levels of MPTM and HPTM were −3.17 and −3.31 eV, respectively, while HOMO levels were −5.06 and −4.96 eV, respectively. The incorporation of the electron-rich thiophene moiety into the polymer backbone led to higher LUMO and HOMO levels for thiophene-containing polymers than for fluorene-containing polymers [55]. As a result, MPTM and HPTM showed lower band gaps than MPFM and HPFM. For PSC application, a low-band–gap-polymer is favorable for the absorption of long-wavelength photons, while the unavoidable reduction of the open-circuit voltage (V_{oc}) would occur as compared to the high band-gap polymer [38]. This is because the V_{oc} is related to the energy difference between the LUMO of electron-acceptor and the HOMO of the electron-donor [56,57].

3.4. EL properties of the PLEDs

For the PLED application, the devices were fabricated from the solutions of polymers dissolved in CHO or CHO/THF. Because of the differences in polymer solubility, most of the polymers (MPFM, HPFM, and HPTM) were dissolved in CHO, while the MPTM polymer was dissolved in a co-solvent (CHO/THF 1:1 by volume). The conjugated polymer film-based light-emitting layer was prepared by an optimized spin-coating procedure. Fig. 4 shows the EL spectra

Table 1
Electrochemical properties of the conjugated polymers.

Polymers	E^{ox}_{onset} (V)	UV–Vis onset (nm)	HOMO (eV)	LUMO (eV)	E_g (eV)
MPFM	0.60	625	−5.31	−3.33	1.98
HPFM	0.57	636	−5.28	−3.34	1.94
MPTM	0.35	654	−5.06	−3.17	1.89
HPTM	0.25	751	−4.96	−3.31	1.65

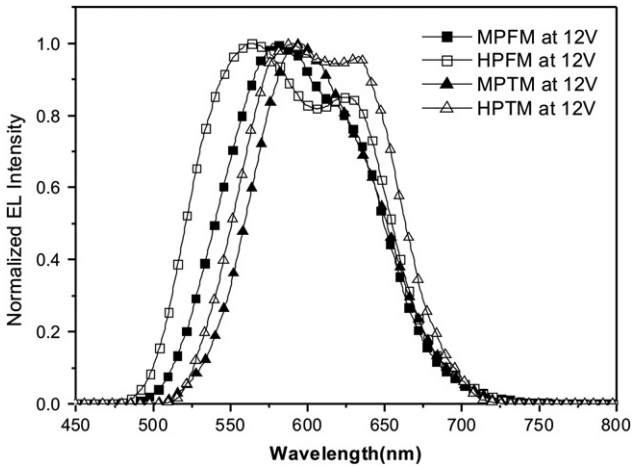

Fig. 4. Normalized EL spectra of the conjugated polymer-based devices (applied voltage: 12 V).

of the PLEDs under an applied voltage (12 V). The EL emission maximum wavelengths, FWHMs of EL, and Commission Internationale de L'Eclairage CIE(x,y) coordinates of the PLEDs are summarized in Table 2. For the fluorene/PM-containing polymer MPFM-based device, the EL spectrum shows a main emission peak at around 578 nm, accompanied by a shoulder emission at around 620 nm. Moreover, the emission maximum of EL was observed at around 597 nm for the thiophene/PM-containing polymer MPTM-based device, with a 20 nm red-shift from the EL of the MPFM-based device. The MPTM with a low band-gap moiety (thiophene) shows a longer EL emission maximum than the MPFM-based device. Unlike the EL emission band of MPFM-based device, no shoulder emission was observed for the MPTM-based device. This demonstrates that the thiophene/PM-containing polymer chains were not inclined to aggregate in solid film as compared to the fluorene/PM-containing polymer chains. Therefore, no shoulder or excimer emission was observed for the MPTM-based device. On the other hand, EL spectra with two emission peaks were observed for the triazine-branched polymer-based devices. The HPFM-based device shows a main emission peak at around 562 nm, accompanied by a shoulder emission at around 625 nm. Maximal EL emission wavelength of the HPFM-based device was shorter than the MPFM-based device. The shorter emission wavelength of the HPFM-based device can be explained by the short conjugation length of the chain segment between the two branching units. Moreover, the shoulder emission peak at around 625 nm was attributed to the excimer emission due to PM aggregation. The co-planarity of the triazine and conjugated chains promotes the

Table 2
Thin-film thickness and EL properties of the conjugated polymer-based devices.

Devices	d[a] (nm)	λ_{max}^{EL} (nm)	FWHM[b] of EL at 12 V	CIE (x,y)[c] at 12 V	Max luminance[d] (cd/m^2)	Max efficiency[e] (cd/A)
MPFM	72	578	110	(0.52,0.47)	865	1.57
HPFM	67	562	134	(0.48,0.56)	1031	1.97
MPTM	66	597	91	(0.56,0.43)	162	0.82
HPTM	73	590	112	(0.56,0.44)	588	0.77

[a] d: Thickness of light emitting layer.
[b] FWHM: Full width at half-maximum of EL.
[c] CIE (x, y): Commission Internationale de L'Eclairage coordinates.
[d] MPFM and HPFM : max luminance observed at 9.5 V; MPTM and HPTM: max luminance observed at 11.5 V.
[e] MPFM: max efficiency observed at 8 V; HPFM: max efficiency observed at 7 V; MPTM: max efficiency observed at 9 V; HPTM: max efficiency observed at 8 V.

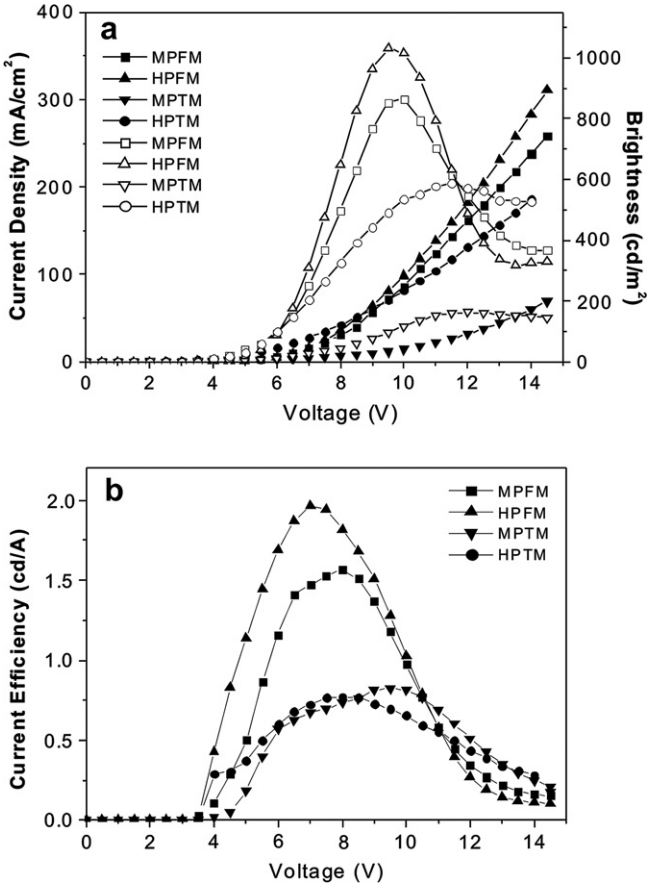

Fig. 5. Current density, brightness, and current efficiency versus applied voltage of the conjugated polymer-based devices (open symbols: brightness; filled symbols: current density and current efficiency).

stacking aggregation of the HPFM. Because of that, an enhancement of the FWHM was observed for the triazine-branched polymer-based device as compared to the main-chain polymer-based device. For the HPTM-based device, two emission peaks were observed at 590 and 633 nm, respectively. A 30 nm red-shift of emission maximum peak was observed for the HPTM-based device as compared to the HPFM-based device. According to the EL spectra, orange-red emission was observed for the fluorene/PM or thiophene/PM-containing polymer-based devices. An orange-red emission polymer with such a broadened EL emission band has potential for application in white-emission PLEDs. High color-purity white emission may be possible for a device based on an appropriate blend of a blue emission polymer and these orange-red emission polymers [58].

The current density, brightness, and current efficiency versus applied voltage of conjugated polymer-based devices are shown in Fig. 5. The maximum brightness and current efficiency of the PLEDs are summarized in Table 2. The results indicate that higher brightness and larger current efficiency were observed for the devices based on fluorene/PM-containing polymers as compared to the devices based on thiophene/PM-containing polymers. This is due to the fact that the polymers with alkyfluorene segments have a higher fluorescence quantum efficiency than the polymers with thiophene segments [20,59]. Moreover, better EL performances were observed for the device based on the triazine-branched polymer in comparison with the device based on the main-chain polymer. For the triazine-branched polymer HPFM-based device, brightness as high as 1031 cd/m^2 and a current efficiency of 1.97 cd/A could be

achieved. In most conjugated polymers, hole-mobility is higher than electron-mobility. The incorporation of a π-deficient triazine was favorable for the balancing of charge injection and transport properties. Therefore, better EL performance was observed for the triazine-branched polymer-based device compared to the main-chain polymer-based device. In spite of this, the current density and brightness of the MPTM-based device were much lower than in the other polymer-based devices. This is due to the poor solubility and thin film quality of the MPTM. The surface morphology of the conjugated polymer-based light-emitting layer was studied using AFM spectroscopy. Our observations indicated that the polymer chains are aggregated, with some area protruding from the thin film surface for the MPTM-based light-emitting layer. Irregular surface morphology of MPTM thin film results in poor contact between the light emitting layer and cathode; this is unfavorable for electron injection from the cathode. As a result, low current density and low brightness were observed for the MPTM-based device. However, the solubility and thin film quality were improved for the HPTM as compared to the MPTM due to the incorporation of the triazine units. Therefore, better EL performances were observed for the HPTM-based device as compared to the device based on MPTM.

3.5. Optical properties of conjugated polymer/PCBM-based composite films

The normalized UV–vis absorption spectra of MPTM/PCBM and HPTM/PCBM composite films with various weight ratios are shown in Fig. 6. The absorption band of the conjugated polymer ranged from 350 to 550 nm, while the absorption band of PCBM ranged from 300 to 375 nm. The maximal absorption peaks of the conjugated polymer and PCBM are observed at around 450 and 325 nm, respectively. Moreover, the absorption intensity of the conjugated polymer was reduced as the PCBM contents increased for the conjugated polymer/PCBM-based composite films. Similar absorption behavior was observed for the fluorene/PM-containing polymer (MPFM and HPFM) based composite films. From a photon-absorption viewpoint, employing less PCBM in the photoactive layer is preferred. However, a typical stoichiometry of a polymer/PCBM blend is 1:4 by weight, which has been found to be optimal for devices in several PSC systems [41]. A high proportion of PCBM limits optical absorption in the composite layer because the PCBM absorption is quite inefficient in the visible region. In addition, the PL spectra of the conjugated polymer/PCBM-based composite films are shown in Fig. 7. The results indicate that the PL emission was almost completely quenched as the polymer and PCBM weight ratio approached 1:1. In the photoactive layer, excitons generated by absorbed photons recombine or dissociate to free-charge carriers (electrons and holes). An efficient free-charge generation must be accompanied by PL quenching, which is a basic requirement for preparing a PSC with excellent PV performance.

3.6. PV properties of the conjugated polymer/PCBM composite-based PSCs

For the PSC application, the cells were fabricated from a solution of polymer/PCBM blend dissolved in CHO or CHO/THF. Most of the polymer (MPFM, HPFM, and HPTM)/PCBM blends were dissolved in CHO, while the MPTM/PCBM blend was dissolved in a co-solvent (CHO/THF, 1:1 by volume). The polymer/PCBM composite film-based photoactive layers were prepared by an optimized spin-coating procedure. The conjugated polymer/PCBM composite-based photoactive layers were thermally treated at 80 °C for 1 h. The photocurrent density versus voltage of the PSCs fabricated from the conjugated polymer/PCBM composite films with various weight ratios are shown in Fig. 8. The PV properties of these PSCs

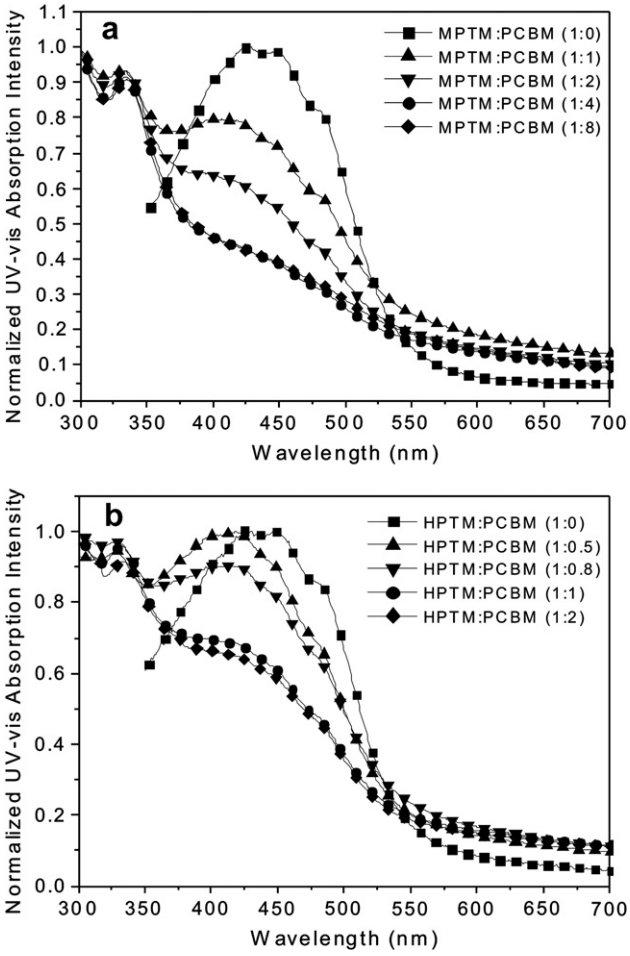

Fig. 6. Normalized UV–vis absorption spectra of the MPTM/PCBM- and HPTM/PCBM-based composite films.

including V_{oc}, short circuit current density (J_{sc}), fill factor (FF), and photo-energy conversion efficiency (η) are summarized in Table 3. For the MPFM/PCBM-based PSCs (PSC I-1–PSC I-4), the values of J_{sc} and η increased with increasing PCBM content, while the values of V_{oc} and FF did not change significantly with the variation of PCBM content. Higher concentrations of PCBM favor the formation of a phase-separated interpenetrating network with sizable domains

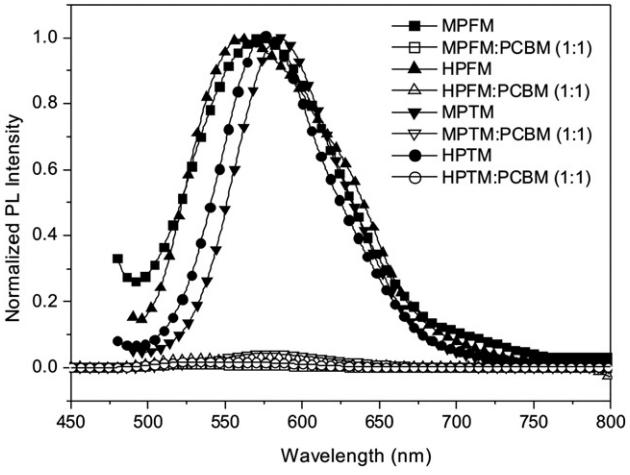

Fig. 7. PL spectra of the conjugated polymer/PCBM-based composite films.

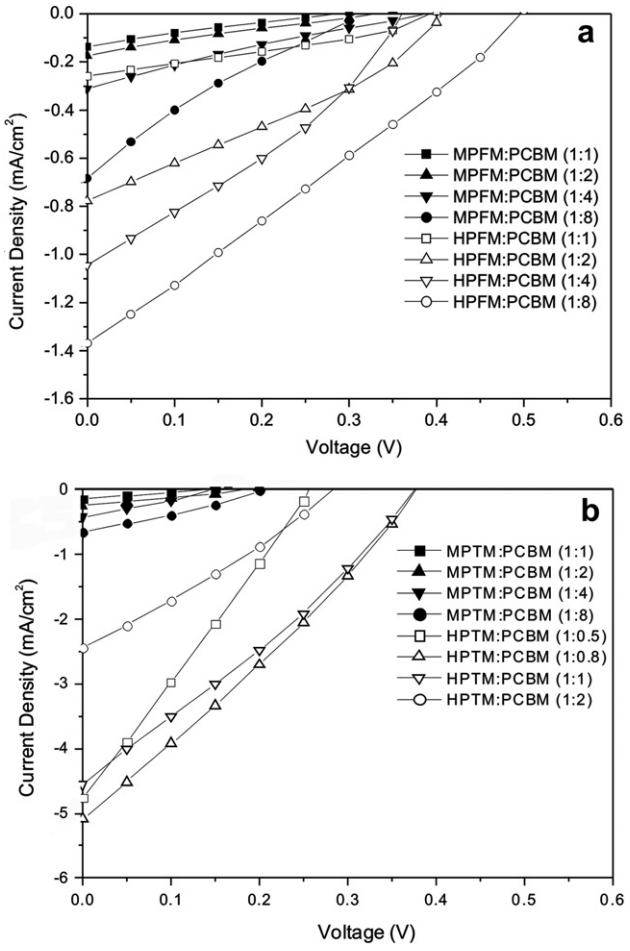

Fig. 8. Current density versus voltage of PSCs fabricated from the conjugated polymer/PCBM composite films with different weight ratios.

in the photoactive layer [60,61], which in turn favors effective charge separation [62,63]. Higher J_{sc} and η values were therefore observed. Moreover, better PV performances were observed for the HPFM/PCBM composite film-based PSCs (PSC II-1 – PSC II-4) as compared to the MPFM/PCBM composite film-based PSCs. The incorporation of the electron-deficient triazine unit led to a lower band gap of HPFM. A low-band-gap-polymer is favorable for the absorption of long-wavelength photons. Moreover, the higher HOMO level would promote hole-injection from the HPFM to HTM layer. As a result, a stronger absorption of solar light and a lower series resistivity of the photoactive layer were responsible for the higher J_{sc}, FF, and η values of the HPFM/PCBM-based PSCs as compared to the MPFM/PCBM-based PSCs. Furthermore, the V_{oc} of the HPFM/PCBM-based PSCs was only slightly larger than that of the MPFM/PCBM-based PSCs. This is because the V_{oc} was mainly determined by the energy difference between the LUMO of electron-acceptor (PCBM) and the HOMO of the electron-donor (conjugated polymer) [57,58]. On the other hand, PSCs based on the thiophene-containing polymer, MPTM, with a narrow energy band gap, were expected to exhibit better PV performances than the fluorene-containing polymer (MPFM) based PSCs. However, lower values of J_{sc} and η were observed for the MPTM/PCBM composite-based PSCs (PSC III-1–PSC III-4) as compared to the MPFM/PCBM-based PSCs. This is due to the poor solubility of MPTM. Poor solubility led to the aggregation of polymer chains and high surface roughness of the solid film. Consequently, low charge mobility in the photoactive layer, and poor contact at the interface of the photoactive layer and cathode were observed. Poor contact hinders electron transport from the photoactive layer to the cathode. Therefore, low values of J_{sc} and η were observed for the MPTM/PCBM-based PSCs. Moreover, the V_{oc} values of the PSCs based on the MPTM/PCBM composite were much lower than the PSCs fabricated from MPFM/PCBM composites. In addition to the poor contact between the photoactive layer and the cathode, an unavoidable reduction of the V_{oc} would occur for the low band-gap polymer (MPTM) as compared to the high band-gap polymer (MPFM) [38]. Furthermore, HPTM/PCBM composite-based PSCs (PSC IV-1–PSC IV-4) exhibited the best PV performance among all of the polymer-based PSCs. J_{sc} and η values of the HPTM/PCBM composite-based PSCs were much higher than those of the other polymer-based PSCs. J_{sc} and η values as high as 5.07 mA/cm^2 and 0.50%, respectively, could be achieved. For the HPTM/PCBM composite-based PSCs, the largest J_{sc} and η values were observed when an optimum weight ratio of HPTM and PCBM was 1:0.8. However, the PV performances would be reduced if higher PCBM contents were further incorporated in the photoactive layer. As higher PCBM content was incorporated, PCBM would aggregate and some areas protruded from the surface of the HPTM/PCBM-based photoactive layer [34]. This results in worse contact between the photoactive layer and cathode. Therefore, the PV performances of the PSCs were reduced. In addition, lower PCBM content was used to obtain better PV performances for the HPTM/PCBM composite-based PSCs as compared to the other polymer-based PSCs. This might be attributed to the higher HOMO level of HPTM than the other conjugated polymers. HPTM, with a higher HOMO level, was favorable for an efficient hole-injection from the photoactive layer to the HTM layer. According to the literature, the electron-mobility of PCBM is 4000 times higher than the hole-mobility in the pure conjugated polymer [64,65]. Moreover, the ratio between the electron-mobility and hole-mobility is only a factor of ten in the polymer/PCBM blend film, resulting in a more balanced charge transport [66]. The hole-mobility and charge balance seems to be enhanced by incorporation of PCBM into the polymer composite [42]. Therefore, HPTM, with high hole-transporting capacity, requires lower PCBM content to achieve the best PV performance.

Table 3
PV properties of the conjugated polymer/PCBM composite film-based PSCs.

PSCs	Polymer: PCBM (w/w)[a]	Roughness (nm)	Thickness (nm)	V_{oc} (V)	J_{sc} (mA/cm^2)	FF	η (%)
PSC I1	MPFM:PCBM (1:1)	0.28	125.3	0.28	0.17	20.6	0.010
PSC I2	MPFM:PCBM (1:2)	0.29	120.1	0.33	0.18	20.2	0.012
PSC I3	MPFM:PCBM (1:4)	0.32	116.7	0.39	0.31	20.4	0.025
PSC I4	MPFM:PCBM (1:8)	0.45	104.1	0.32	0.69	21.1	0.047
PSC II1	HPFM:PCBM (1:1)	0.29	121.8	0.39	0.26	28.4	0.029
PSC II2	HPFM:PCBM (1:2)	0.30	115.3	0.40	0.78	28.3	0.088
PSC II3	HPFM:PCBM (1:4)	0.35	94.7	0.36	1.05	29.7	0.113
PSC II4	HPFM:PCBM (1:8)	0.39	90.3	0.49	1.37	26.5	0.178
PSC III1	MPTM:PCBM (1:1)	1.88	119.5	0.15	0.14	22.2	0.005
PSC III2	MPTM:PCBM (1:2)	2.05	110.7	0.18	0.25	26.1	0.012
PSC III3	MPTM:PCBM (1:4)	2.63	96.6	0.16	0.42	28.0	0.019
PSC III4	MPTM:PCBM (1:8)	2.89	87.5	0.20	0.65	29.9	0.039
PSC IV1	HPTM:PCBM (1:0.5)	0.29	112.3	0.25	4.77	26.0	0.311
PSC IV2	HPTM:PCBM (1:0.8)	0.33	111.7	0.37	5.07	26.7	0.500
PSC IV3	HPTM:PCBM (1:1)	0.38	110.1	0.37	4.58	26.8	0.454
PSC IV4	HPTM:PCBM (1:2)	0.37	100.8	0.28	2.45	27.1	0.186

[a] Polymer/PCBM composite films: annealing at 80 °C for 1 h.

3.7. Morphology of conjugated polymer/PCBM-based composite films

Recently, it has been reported that the PV properties of PSCs can be improved by manipulating the morphology within the

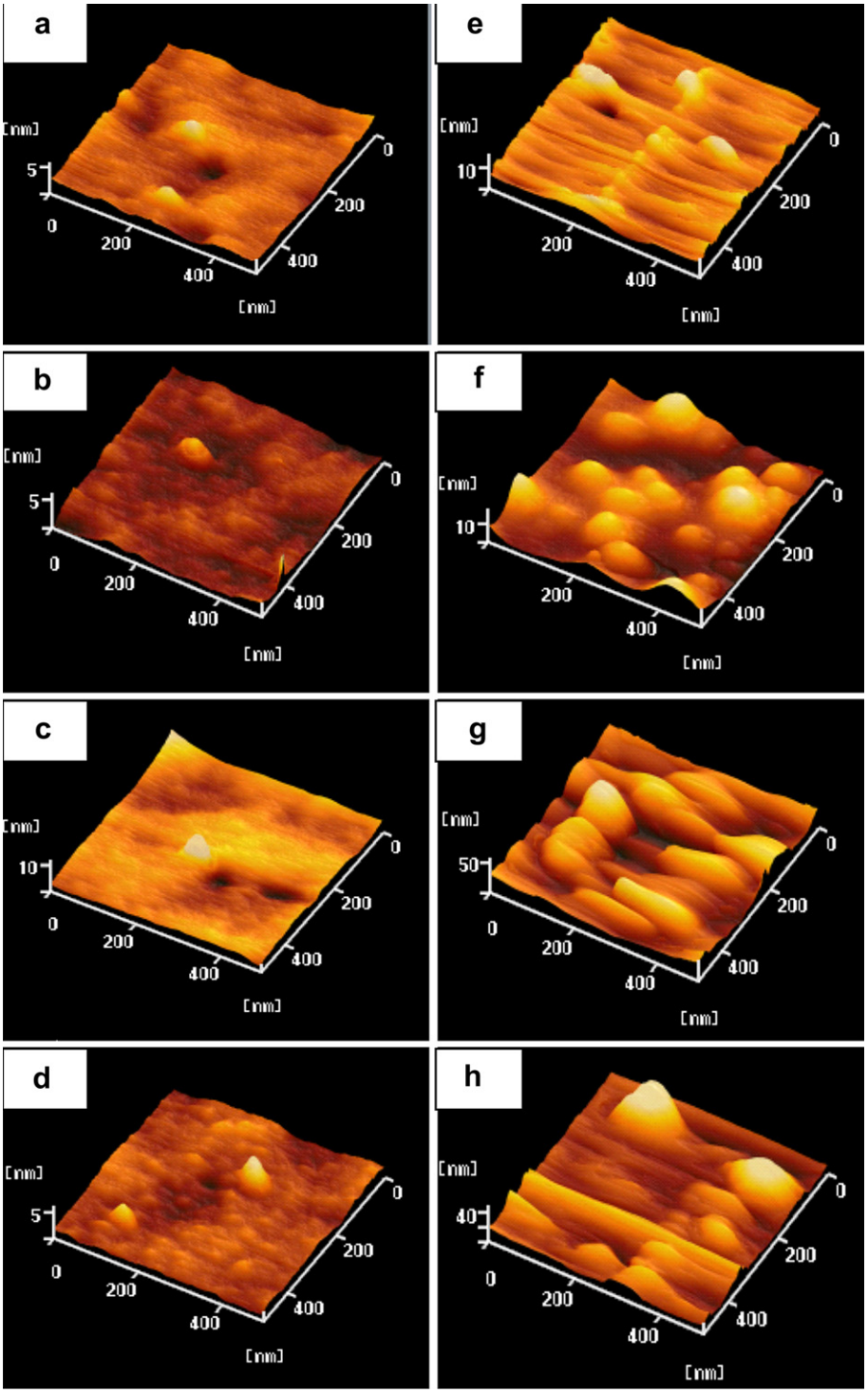

Fig. 9. AFM spectra of MPFM/PCBM (1:8 w/w) and MPTM/PCBM (1:8 w/w) composite films after drying under different conditions ((a) MPFM/PCBM: in a vacuum system, 24 h; (b) MPFM/PCBM: 80 °C, 1 h; (c) MPFM/PCBM: 120 °C, 10 min; (d) MPFM/PCBM: 120 °C, 60 min; (e) MPTM/PCBM: in a vacuum system, 24 h; (f) MPTM/PCBM: 80 °C, 1 h; (g) MPTM/PCBM: 120 °C, 10 min; (h) MPTM/PCBM: 120 °C, 60 min).

photoactive polymer blend [35,44,45]. The compatibility and morphology of the conjugated polymer/PCBM composite films was investigated using AFM microscopy. Figs. 9 and 10 show the AFM micrographs of the MPFM/PCBM, MPTM/PCBM and HPTM/PCBM composite films after being dried in a vacuum system or annealed at elevated temperatures for different times. The roughness of the composite films is summarized in Table 4. As shown in Fig. 9, the MPFM/PCBM composite film shows very smooth surface morphology, while the MPTM/PCBM composite film shows large-scale aggregation. In particular, the MPTM/PCBM composite film annealed at 120 °C is characterized by large agglomerates extending over one hundred nanometers with accompanying high surface roughness. This observation indicates that MPTM has a poor compatibility with PCBM. This

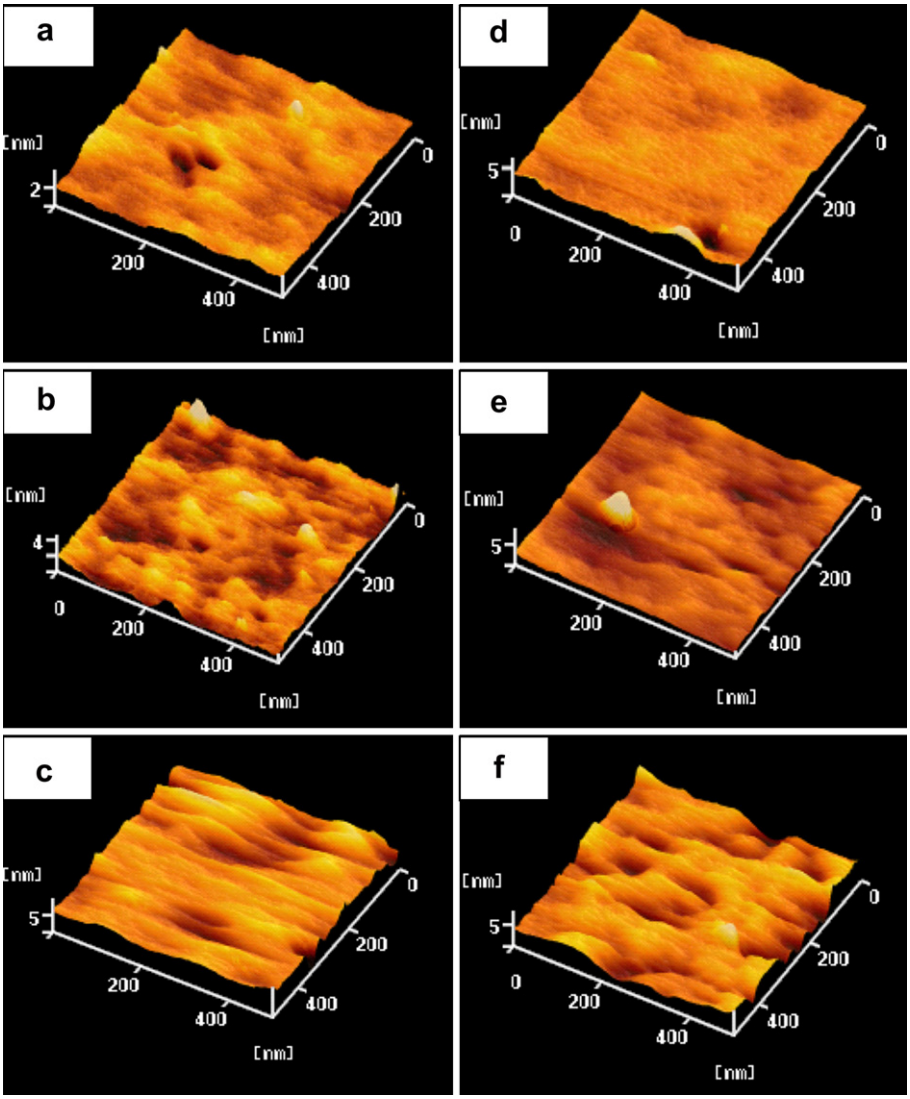

Fig. 10. AFM spectra of HPTM/PCBM (1:0.8 w/w) composite films after drying under different conditions ((a) in a vacuum system, 24 h; (b) 80 °C, 1 h; (c) 120 °C, 10 min; (d) 120 °C, 30 min; (e) 120 °C, 1 h; (f) 120 °C, 3 h).

agglomeration is likely due to the poor solubility of MPTM in CHO/THF. Moreover, the agglomeration became more pronounced with increasing annealing time. In addition, the same surface morphology was observed for the HPFM/PCBM composite film as compared to the MPFM/PCBM composite film. The surface morphologies of HPTM/PCBM composite films dried at different processing conditions are shown in Fig. 10. The polymer films dried in the vacuum system or annealed at 80 °C show a smoother surface than the polymer film annealed at 120 °C. The high roughness of the HPTM/PCBM composite film annealed at 120 °C was attributed to the rapid removal of the organic solvent. Moreover, the roughness of the polymer film was reduced when the annealing time was increased from 10 min to 30 min. However, further increasing the annealing time from 1 h to 3 h exacerbated the roughness. This increase in surface roughness can be attributed to the reorientation or aggregation of polymer chains in the HPTM/PCBM composite film after annealing at elevated temperature for 3 h. We concluded that the surface roughness and morphology of the polymer/PCBM composite film were determined by the polymer solubility and annealing conditions of the polymer film.

3.8. Thermal annealing effect on the PV properties of the PSCs

The photocurrent density versus voltage for the PSCs fabricated from the conjugated polymer/PCBM composite films dried in a vacuum system or annealed at elevated temperatures are shown in Figs. 11 and 12. The PV properties of these PSCs are summarized in Table 4. For the MPFM/PCBM composite film-based PSCs, better PV properties were observed for the PSCI4, based on the composite film annealed at 80 °C for 1 h, as compared to the PSCI4-V, based on the composite film dried in the vacuum system for 24 h, even though the annealed polymer film has a higher roughness. As the polymer chains reoriented during the thermal annealing process, the compatibility between the polymer and PCBM was enhanced and a phase-separated interpenetrating network with sizable domains was formed in the photoactive layer. Consequently, better PV properties of the PSC were observed. For the other polymer-based PSCs, better PV properties were also observed for the composite film annealed at 80 °C as compared to the composite film dried in the vacuum system. The PSCs fabricated from the polymer/PCBM composite film annealed at 120 °C for different times were also studied. For all of the

Table 4
Thermal annealing effect on the PV performances of the PSCs.

PSCs[a]	Temperature (°C)/time (min)[b]	Roughness (nm)	V_{oc} (V)	J_{sc} (mA/cm^2)	FF	η (%)
PSCI4-V	Vac./24 h	0.36	0.18	0.56	29.2	0.029
PSCI4	80 °C/60	0.45	0.32	0.69	21.1	0.047
PSCI4-1	120 °C/10	0.73	0.15	0.63	32.5	0.031
PSCI4-2	120 °C/30	0.48	0.38	0.65	24.7	0.061
PSCI4-3	120 °C/60	0.34	0.20	0.63	26.5	0.033
PSCII4-V	Vac./24 h	0.30	0.38	1.04	26.0	0.103
PSCII4	80 °C/60	0.39	0.49	1.37	26.5	0.178
PSCII4-1	120 °C/10	0.52	0.24	0.87	29.8	0.062
PSCII4-2	120 °C/30	0.43	0.28	1.06	29.1	0.086
PSCII4-3	120 °C/60	0.36	0.20	0.79	31.2	0.050
PSCIII4-V	Vac./24 h	1.00	0.18	0.35	26.9	0.017
PSCIII4	80 °C/60	2.89	0.20	0.65	29.9	0.039
PSCIII4-1	120 °C/10	7.46	0.18	0.95	27.1	0.046
PSCIII4-2	120 °C/30	6.35	0.20	0.96	27.5	0.053
PSCIII4-3	120 °C/60	5.29	0.21	0.65	29.9	0.041
PSCIV2-V	Vac./24 h	0.24	0.33	4.14	27.7	0.378
PSCIV2	80 °C/60	0.33	0.37	5.07	26.7	0.500
PSCIV2-1	120 °C/10	0.72	0.42	4.50	31.1	0.587
PSCIV2-2	120 °C/30	0.30	0.43	3.35	34.4	0.496
PSCIV2-3	120 °C/60	0.42	0.41	2.56	28.6	0.300

[a] Composition of photoactive layer: PSCI4-V – PSCI4-3: MPFM/PCBM = 1: 8; PSCII4-V – PSCII4-3: HPFM/PCBM = 1: 8; PSCIII4-V – PSCIII4-3: MPTM/PCBM = 1: 8; PSCIV4-V – PSCIV4-3: HPTM/PCBM = 1: 0.2.

[b] Thermal treated conditions of photoactive layer: drying in a vacuum system or thermal annealing at various temperatures for different times.

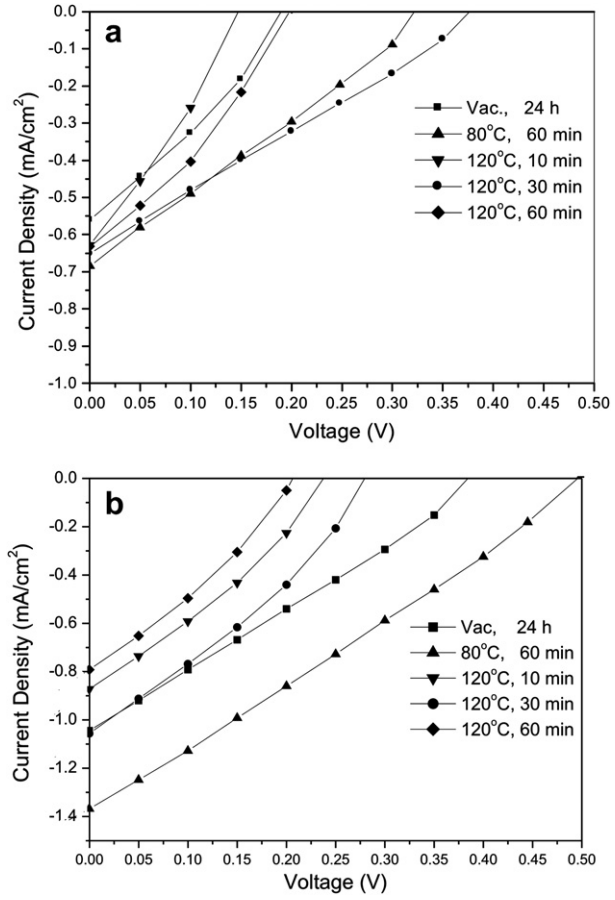

Fig. 11. Current density versus voltage of PSCs fabricated from the MPFM/PCBM (1:8 w/w) and HPFM/PCBM (1:8 w/w) composite films after drying in a vacuum system or thermal annealing at various temperatures for different times.

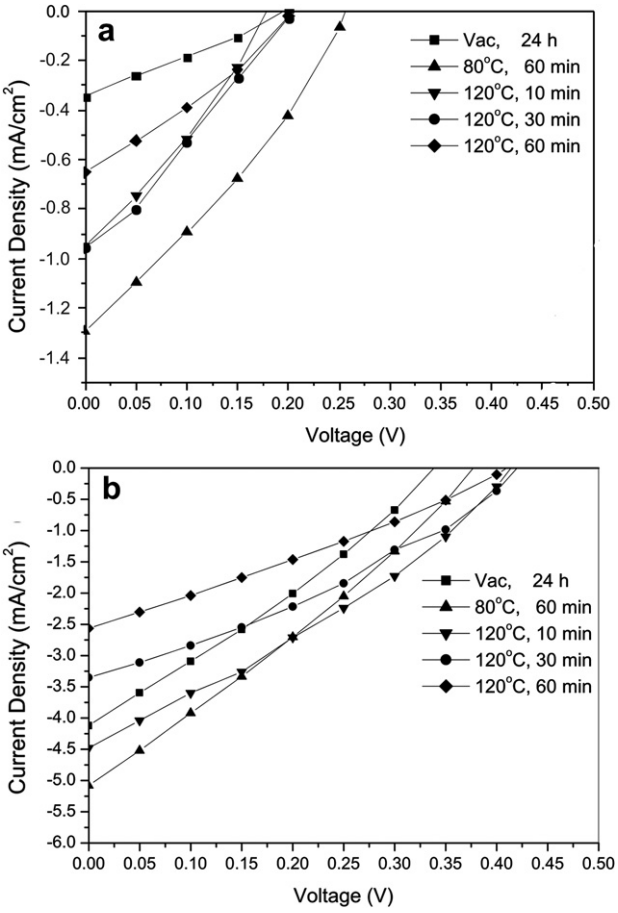

Fig. 12. Current density versus voltage of PSCs fabricated from the MPTM/PCBM (1:8 w/w) and HPTM/PCBM (1:0.8 w/w) composite films after drying in a vacuum system or thermal annealing at various temperatures for different times.

conjugated polymer/PCBM composite films, much higher surface roughness was observed in the film annealed at 120 °C for 10 min than in the film annealed at 80 °C for 1 h. High surface roughness led to poor contact at the interface between the photoactive polymer film and the cathode, resulting in the small V_{oc} and low J_{sc} values of the PSCs fabricated from the polymer films annealed at 120 °C for 10 min. Moreover, the optimized thermal annealing time was 30 min for the MPFM/PCBM, HPFM/PCBM, and MPTM/PCBM composite films, expect for the HPTM/PCBM composite film. For the MPFM/PCBM and HPFM/PCBM composite films, the annealing temperature (120 °C) was near the glass transition temperatures of the MPFM/PCBM (about 127 °C) and HPFM/PCBM (about 131 °C) composite. The polymer chains would thus reorient during the thermal annealing process. The surface roughness of the composite films was reduced with increasing thermal annealing time. Better contact at the interface of photoactive layer and cathode was observed. The compatibility between the polymer and PCBM was also improved. Consequently, improved PV properties were observed for the PSCI4-2 and PSCII4-2 as compared to the PSCI4-1 and PSCII4-1. However, the PV properties of PSCI4-3 and PSCII4-3 were reduced as the annealing time of the polymer composite films increased above 60 min. This can be attributed to the aggregation of the polymer chains as the annealing time was increased. Although aggregation of the MPFM (or HPFM) polymer chains was not observed by the AFM spectra as clearly as for MPTM, the polymer chain aggregation was proved by the PL spectra. A red-shifting and an FWHM enhancement of

the PL emission peak evidenced the aggregate formation in the thermally annealed polymer films. As a result, the charge mobility through the polymer chains would be suppressed. The PV properties of PSCI4-3 and PSCII4-3 were therefore reduced. Furthermore, the influence of thermal annealing time on the PV properties of MPTM/PCBM composite film-based PSCs was the same as the MPFM/PCBM and HPFM/PCBM composite film-based PSCs. The PV properties of PSC III4-2 were better than PSC III4-1 and PSC III4-3. Since the thermal annealing temperature (120 °C) was higher than the T_g (109 °C) of the MPTM/PCBM composite, the agglomeration in the polymer film became pronounced with increasing annealing time. The agglomeration sizes of 100 nm are much larger than the exciton diffusion length (10–20 nm), so that many excitons recombine before reaching the hetero-interface, thus limiting the PV properties of MPTM/PCBM composite film-based PSCs [67]. Poor PV properties were observed for PSCs fabricated from the MPTM/PCBM composite film annealed at 120 °C. On the other hand, the PV properties were worsened with increasing annealing time for the PSCs (PSC IV2-1–PSC IV2-3) fabricated from the HPTM/PCBM composite films annealed at 120 °C. This can be attributed to the morphology modification of the HPTM/PCBM composite film. Since the annealing temperature (120 °C) was higher than the T_g (106 °C) of the polymer composite, the molecular morphology changed significantly with increasing annealing time. The best PV properties were observed for the PSC IV2-1 as compared to the PSC IV2-2 and PSC IV2-3, even though higher surface roughness of the photoactive layer was observed for PSC IV2-1. This demonstrated that the PV properties are not only affected by the surface roughness of the photoactive layer, but also by the internal molecular morphology of the polymer/PCBM composite.

4. Conclusions

A series of main-chain type and triazine-branched fluorene and thiophene copolymers containing a 2-pyran-4-ylidene-malononitrile derivative were developed for PLED and PSC applications. For PLED application, higher brightness and larger current efficiency were observed for the devices based on fluorene/PM-containing polymers as compared to the devices based on thiophene/PM-containing polymers. Moreover, the incorporation of a π-deficient triazine was favorable for the balancing of charge injection and transport properties in the PLEDs. Better EL performances were observed for the triazine-branched polymer-based device compared to the main-chain polymer-based device. For PSC application, the PV properties of the HPTM/PCBM composite-based PSCs were much better than those of the other polymer/PCBM composite-based PSCs. The incorporation of the electron-deficient triazine unit led to the lower LUMO level and the higher HOMO level of HPTM than MPTM. The low-band-gap-polymer was favorable for the absorption of long-wavelength photons. Moreover, the higher HOMO level promoted the hole-injection from the HPTM to the hole-transport layer. As a result, a stronger absorption intensity of solar light and a lower series resistivity of the photoactive layer were responsible for the improved PV properties of the HPTM/PCBM-based PSCs as compared to those of the other polymer/PCBM-based PSCs. In addition, thermal annealing effects on the morphology of the photoactive layer and the PV properties of the PSCs were also studied. Since the polymer chains would reorient during the thermal annealing process, and therefore enhance the compatibility between the polymer and PCBM, this resulted in the formation of a phase-separated interpenetrating network with sizable domains in the photoactive layer. The best PV properties were observed for the PSCs fabricated from the polymer/PCBM composite film annealed at elevated temperature.

Acknowledgment

The authors thank the National Science Council of Taiwan, ROC, for financial support (Grant NSC98-2221-E-224-001)

References

[1] Kobayashi H, Kanbe S, Seki S, Kigchi H, Kimura M, Yudasaka I, et al. A novel RGB multicolor light-emitting polymer display. Synthetic Metals 2000;111–112:125–8.
[2] Lee RH, Lin KT, Huang CY. High red, green, andblue color purity electroluminescence from MEH-PPV and polyalkyfluorenes-based bright white polymer light emitting displays. Journal of Polymer Science, Part B: Polymer Physics 2007;45:330–41.
[3] Yu G, Gao J, Hummelen JC, Wudl F, Heeger AJ. Polymer photovoltaic cells: enhanced efficiencies via a network of internal donor-acceptor hetero-junctions. Science 1995;270:1789–91.
[4] Halls JJM, Pichler K, Friend RH, Moratti SC, Holmes AB. Exciton diffusion and dissociation in a poly(*p*-phenylenevinylene)/C_{60} heterojunction photovoltaic cell. Applied Physics Letters 1996;68:3120–2.
[5] Abdalla TA, Mammo W, Workalemahu B. Electronic and photovoltaic properties of a single layer poly[3-(2″ 5″-diheptyloxyphenyl)-2,2′-bithiophene] devices. Synthetic Metals 2004;144:213–9.
[6] Tang CW. Two-layer organic photovoltaic cell. Applied Physics Letters 1986;48:183–5.
[7] Alem S, Bettignies RD, Nunzi JM, Cariou M. Efficient polymer-based interpenetrated network photovoltaic cells. Applied Physics Letters 2004;84:2178–80.
[8] Wienk MM, Kroon JM, Verhees WJH, Knol J, Hummelen JC, Hal PAV, et al. Efficient methano [70] fullerene/MDMO-PPV bulk hetero-junction photovoltaic cells. Angewandte Chemie International Edition 2003;42:3371–5.
[9] Duren JKJV, Yang X, Loos J, Lieuwma CWTB, Sieval AB, Hummelen JC, et al. Relating the morphology of poly(p-phenylene vinylene)/methanofullerene blends to solar-cell performance. Advanced Functional Materials 2004;14:425–34.
[10] Brabec CJ, Cravino A, Meissner D, Sariciftci NS, Fromherz T, Rispens MT, et al. Origin of the open circuit voltage of plastic solar cells. Advanced Functional Materials 2001;11:374–80.
[11] Fletcher RB, Lidzey DG, Bradley DDC, Walker S, Inbasekaran M, Woo EP. High brightness conjugated polymer LEDs. Synthetic Metals 2000;111–112:151–3.
[12] Lee RH, Lee YZ, Chao CI. Enhanced performance of polymer light-emitting device via optimization of processing conditions and device configuration. Journal of Applied Polymer Science 2006;100:133–41.
[13] Lee RH, Hsu HF, Chan LH, Chen CT. Synthesis and electroluminescence properties of novel tetraphenylsilane-oxadiazole-diphenyl(*para*-tolyl)amine polymer. Polymer 2006;47:7001–12.
[14] Patra A, Pan M, Friend CS, Lin TC, Cartwright AN, Prasad PN, et al. Electroluminescence properties of systematically derivatized organic chromophores containing electron donor and acceptor groups. Chemistry of Materials 2002;14:4044–8.
[15] Pudzich R, Salbeck J. Synthesis and characterization of new oxadiazoleamine based spiro-linked fluorescence dyes. Synthetic Metals 2003;138:21–31.
[16] Niu YH, Chen B, Liu S, Yip H, Bardecker J, Jen AKY, et al. Highly efficient red electrophosphorescent devices based on an iridium complex with trifluoromethyl-substituted pyrimidine ligand. Applied Physics Letters 2004;85:1619–21.
[17] Pu YJ, Kurata T, Soma M, Kido J, Nishide H. Triphenylamine- and oxadiazole-substituted poly(1,4-phenylenevinylene)s: synthesis, photo-, and electroluminescent properties. Synthetic Metals 2004;143:207–14.
[18] Grimsdale AC, Leclere P, Lazzaroni R, Mackenzie JD, Murphy C, Setayesh S, et al. Correlation between molecular structure, microscopic morphology, and optical properties of poly(tetraalkylindenofluorene)s. Advanced Functional Materials 2002;12:729–33.
[19] Sung HH, Lin HC. Novel alternating fluorene-based conjugated polymers containing oxadiazole pendants with various terminal groups. Macromolecules 2004;37:7945–54.
[20] Kreyenschmidt M, Klaerner G, Fuhrer T, Ashenhurst J, Karg S, Chen WD, et al. Thermally stable blue-light-emitting copolymers of poly(alkylfluorene). Macromolecules 1998;31:1099–103.
[21] Zeng G, Yu WL, Chua SJ, Huang W. Spectral and thermal spectral stability study for fluorene-based conjugated polymers. Macromolecules 2002;35:6907–14.
[22] Jacob J, Zhang J, Grimsdale AC, Mullen K, Gaal M, List EJW. Poly (tetraarylindenofluorene)s: new stable blue-emitting polymers. Macromolecules 2003;36:8240–5.
[23] Kulkarni AP, Jenekhe SA. Blue light-emitting diodes with good spectral stability based on blends of poly(9,9-dioctylfluorene): interplay between morphology, photophysics, and device performance. Macromolecules 2003;36:5285–96.
[24] Xiao S, Nguyen M, Gong X, Cao Y, Wu H, Moses D, et al. Stabilization of semiconducting polymers with silsesquioxane. Advanced Functional Materials 2003;13(1):25–9.
[25] Lin WJ, Chen WC, Wu WC, Niu YH, Jen AKY. Synthesis and optoelectronic properties of starlike polyfluorenes with a silsesquioxane core. Macromolecules 2004;37:2335–41.

[26] Lee J, Cho HJ, Jung BJ, Cho NS, Shim HK. Stabilized blue luminescent polyfluorenes: introducing polyhedral oligomeric silsesquioxane. Macromolecules 2004;37:8523–9.
[27] Chou CH, Hsu SL, Dinakaran K, Chiu MY, Wei KH. Synthesis and characterization of luminescent polyfluorenes incorporating side-chain-tethered polyhedral oligomeric silsesquioxane units. Macromolecules 2005;38:745–51.
[28] Liu XM, He C, Hao XT, Tan LW, Li Y, Ong KS. Hyperbranched blue-light-emitting alternating copolymers of tetrabromoarylmethane/silane and 9,9-dihexylfluorene-2,7-diboronic acid. Macromolecules 2004;37:5965–70.
[29] Liu XM, Xu J, Lu X, He C. Novel glassy tetra(N-alkyl-3-bromocarbazole-6-yl)silanes as building blocks for efficient and nonaggregating blue-light-emitting tetrahedral materials. Organic Letters 2005;7:2829–32.
[30] Liu XM, He C, Huang J, Xu J. Highly efficient blue-light-emitting glass-forming molecules based on tetraarylmethane/silane and fluorene: synthesis and thermal, optical, and electrochemical properties. Chemistry of Materials 2005;17:434–41.
[31] Wen GA, Xin Y, Zhu XR, Zeng WJ, Zhu R, Feng JC, et al. Hyperbranched triazine-containing polyfluorenes: efficient blue emitters for polymer light-emitting diodes. Polymer 2007;48:1824–9.
[32] Chen ACA, Wallace JU, Wei SKH, Zeng L, Chen SH, Blanton TN. Light-emitting organic materials with variable charge injection and transport properties. Chemistry of Materials 2006;18:204–13.
[33] Lee RH, Chen WS, Wang YY. Synthesis and electroluminescence properties of novel hyper-branched light emitting polymers. Thin Solid Films 2009;517:5747–56.
[34] Padinger F, Rittberger RS, Sariciftci NS. Effects of postproduction treatment on plastic solar cells. Advanced Functional Materials 2003;13:85–8.
[35] Ma W, Yang C, Gong X, Lee K, Heeger AJ. Thermally stable, efficient polymer solar cells with nanoscale control of interpenetrating nework morphology. Advanced Functional Materials 2005;15:1617–22.
[36] Erb T, Zhokhavets U, Gobsch G, Raleva S, Stuhn B, Schilinsky P, et al. Correlation between structural and optical properties of composite polymer/fullerene films for organic solar cells. Advanced Functional Materials 2005;15:1193–6.
[37] Colladet K, Nicolas M, Goris L, Lutsen L, Vanderzande D. Low-band gap polymers for photovoltaic applications. Thin Solid Films 2004;451:7–11.
[38] Zhang F, Mammo W, Andersson LM, Admassie S, Andersson MR, Inganas O. Low-bandgap alternating fluorene copolymer/methanofullerene heterojunctions in effcieicnt near-infrared polymer solar cells. Advanced Materials 2006;18:2169–73.
[39] Li YF, Zou YP. Conjugated polymer photovoltaic materials with broad absorption band and high charge carrier mobility. Advanced Materials 2008;20:2952–8.
[40] Hadipour A, Boer BD, Wildeman J, Kooistra FB, Hummelen JC, Turbiez MGR, et al. Solution-processed organic tandem solar cells. Advanced Functional Materials 2006;16:1897–903.
[41] Shaheen SE, Brabec CJ, Sariciftci NS, Padinger F, Fromherz T, Hummelen JC. 2.5% efficient organic plastic solar cells. Applied Physics Letters 2001;78(6):841–3.
[42] Mihailetchi VD, Koster LJA, Blom PWM, Melzer C, Boer BD, Duren JKJV, et al. Compositional dependence of the performance of poly(p-phenylene vinylene): methanofullerene bulk-heterojunction solar cells. Advanced Functional Materials 2005;15:795–801.
[43] Hoppe H, Niggemann M, Christoph Winder, Kraut J, Hiesgen R, Hinsch A, et al. Nanoscale morphology of conjugated polymer/fullerene-based bulk-heterojunction solar cells. Advanced Functional Materials 2004;14(10):1005–11.
[44] Klimov E, Li W, Yang X, Hoffmann GG, Loos J. Scanning near-field and confocal Raman microscopic investigation of P3HT-PCBM systems for solar cell applications. Macromolecules 2006;39:4493–6.
[45] Rait S, Kashyap S, Bhatnagar PK, Mathur PC, Sengupta SK, Kumar J. Effect of a buffer layer, composition and annealing on the performance of a bulk heterojunction polythiophene/fullerene composite photovoltaic device. Physica E 2007;39:191–7.
[46] Kim JH, Lee H. Synthesis, electrochemistry, and electroluminescence of novel red-emitting poly(*p*-phenylenevinylene) derivative with 2-pyran-4-ylidene-malononitrile obtained by the heck reaction. Chemistry of Materials 2002;14:2270–5.
[47] Peng Q, Lu ZY, Huang Y, MG X, Han SH, Peng JB, et al. Synthesis and characterization of new red-emitting polyfluorene derivatives containing electron-deficient 2-pyran-4-ylidene-malononitrile moieties. Macromolecules 2004;37:260–6.
[48] Jianzhong C, Suh HJ, Kim SH. Synthesis and properties of conjugated copolymers with 2-pyran-4-ylidene malononitrile. Dyes and Pigments 2006;68:75–7.
[49] Choa NS, Hwang DH, Jung BJ, Ohc J, Chuc HY, Shima HK. Synthesis and light emitting properties of fluorene–carbazole-based conjugated copolymers. Synthetic Metals 2004;143:277–82.
[50] Guo ZQ, Zhu WH, Xiong YY, Tian H. Multiple logic fluorescent thermometer system based on N-isopropyl-methacrylamide copolymer bearing dicyanomethylene-4H-pyran moiety. Macromolecules 2009;42:1448–53.
[51] Liu B, Zhu WH, Zhang Q, Wu WJ, Xu M, Ning ZJ, et al. Coveniently synthesized isophorone dyes for high efficiency dye-sensitized solar cells: tuning photovoltaic performance by structural modification of donor group in donor-π-acceptor system. Chemical Communications 2009:1766–8.
[52] Miller LL, Nordblom GD, Mayeda EA. A simple, comprehensive correlation of organic oxidation and ionization potentials. Journal of Organic Chemistry 1972;37:916–8.
[53] Yang CJ, Jenekhe SA. Conjugated aromatic polyimines. 2. synthesis, structure, and properties of new aromatic polyazomethines. Macromolecules 1995;28:1180–96.
[54] Sun QJ, Wang HQ, Yang CH, Li YF. Synthesis and electroluminescence of novel block copolymers containing crown ether spacers. Journal of Materials Chemistry 2003;13:800–6.
[55] Lim E, Jung BJ, Shim HK. Synthesis and characterization of a new light-emitting fluorene-thieno[3,2- *b*]thiophene-based conjugated copolymer. Macromolecules 2003;36:4288–93.
[56] Brabec CJ, Cravino A, Meissner D, Sariciftci NS, Rispens NT, Sanchez L, et al. The influence of materials work function on the open circuit voltage of plastic solar cells. Thin Solid Films 2002;403:368–72.
[57] Gadisa A, Svensson M, Andersson MR, Inganas O. Correlation between oxidation potential and open-circuit voltage of composite solar cells based on blends of polythiophenes fullerene derivative. Applied Physics Letters 2004;84:1609–11.
[58] Sun QJ, Hou JH, Yang CH, Li YF, Yang Y. Enhanced performances of white polymer light-emitting diodes using polymer blend as hole-transporting layer. Applied Physics Letters 2006;89:153510.
[59] Barta P, Cacialli F, Friend RH, Zagorska M. Efficient photo and electroluminescence of regioregular poly(alkylthiophene)s. Journal of Applied Physics 1998;84:6279–84.
[60] Sariciftci NS, Smilowitz L, Heeger AJ, Wudl F. Photoinduced electron transfer from a conducting polymer to buckminsterfullerene. Science 1992;258:1474–6.
[61] Yu G, Zhang C, Heeger AJ. Dual-function semiconducting polymer devices: light-emitting and photodetecting diodes. Applied Physics Letter 1994;64:1540–2.
[62] Gao F, Hide F, Wang H. Efficient photodetectors and photovoltaic cells from composites of fullerenes and conjugated polymers: photoinduced electron transfer. Synthetic Metals 1997;84:979–80.
[63] Kim H, Kim JY, Lee K, Park Y, Jin Y, Suh H. Organic photovoltaic cells based on conjugated polymer/fullerene composites. Current Applied Physics 2001;1:139–43.
[64] Mihailetchi VD, Duren JKJV, Blom PWM, Hummelen JC, Janssen RAJ, Kroon JM, et al. Electron transport in a methanofullerene. Advanced Functional Materials 2003;13:43–6.
[65] Blom PWM, Jong MJMD, Munster MJV. Electric-field and temperature dependence of the hole mobility in poly *p*-phenylene vinylene. Physical Review B: Condensed Matter and Materials Physics 1997;55:R656–9.
[66] Melzer C, Koop E, Mihailetchi VD, Blom PWM. Hole transport in poly (phenylene vinylene)/Methanofullerene bulk-heterojunction solar cells. Advanced Functional Materials 2004;14:865–70.
[67] Kietzke T, Shin RYC, Egbe DAM, Chen ZK, Sellinger A. Effect of annealing on the characteristics of organic solar cells: polymer blends with a 2-vinyl-4,5-dicyanoimidazole derivative. Macromolecules 2007;40:4424–8.